analytical chemistry



pubs.acs.org/ac
Article

# Direct Identification and Quantification of Recombinant Adeno-Associated Virus in Crude Cell Lysate and Conditioned Medium by Mass Photometry

Yuki Yamaguchi,[#] Saki Shimojo,[#] Risa Shibuya, Karin Bandoh, Aoba Matsushita, Mitsuko Fukuhara, Yasuo Tsunaka, Tetsuo Torisu, and Susumu Uchiyama*

Cite This: *Anal. Chem.* 2025, 97, 10405−10416
Read Online

ACCESS | Metrics & More | Article Recommendations | Supporting Information

**ABSTRACT:** Recombinant adeno-associated virus (rAAV) has attracted attention as a gene therapy vector. Monitoring the percentage of full particles (FPs) to the sum of empty particles (EPs) and FPs (F/E ratio) is required to optimize the rAAV production conditions; however, there is a lack of analytical methods to identify FPs and EPs and quantify the F/E ratio of rAAV without purification. Here, we established a direct analysis method for identifying FPs and EPs and quantifying the F/E ratio and genomic titer of unpurified rAAV in crude cell lysate and conditioned medium by mass photometry (MP). MP can detect the events of both molecules that bind to the glass surface and molecules that unbind from the glass surface. Few unbinding molecules were detected in the cell lysate and conditioned medium, but unbinding particles were as prevalent as binding particles in rAAV. By analyzing the unbinding side of the histogram, the F/E ratio of rAAV in the cell lysate was directly quantified with accuracy comparable to that of purified rAAV, which showed there was no interference from impurities. The genomic titer of rAAV in cell lysate was also estimated using particle counts of the unbinding side. This method can successfully determine the F/E ratio and estimate genomic titers of rAAV in crude cell lysate and conditioned medium during the manufacturing process. Direct quantification by MP is a convenient, rapid, and accurate method for quantifying unpurified rAAV and will be useful for improving rAAV production processes, for example, by screening manufacturing conditions.

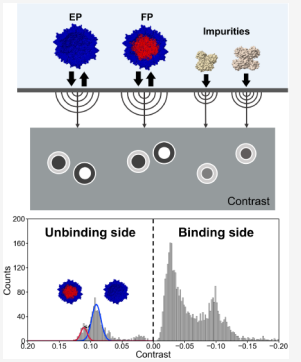


## INTRODUCTION

Recombinant adeno-associated virus (rAAV) is a type of viral vector that has attracted attention as a gene delivery tool in gene therapy. Seven rAAV-based gene therapy products have been approved by the United States Food Drug Administration for treatment of lipoprotein lipase deficiency, inherited retinal disease, spinal muscular atrophy, aromatic L-amino acid decarboxylase deficiency, hemophilia, and Duchenne muscular dystrophy.[1]

rAAVs are usually produced by transfection of three plasmids: an AAV vector plasmid that contains a transgene cassette flanked by AAV inverted terminal repeats (ITRs) (pAAV-GOI), an AAV packaging plasmid that contains AAV Rep and Cap genes for expression of viral proteins (pAAV-RepCap), and a helper plasmid that supplies adenovirus helper genes (pHelper) in human or insect cells (e.g., HEK293 or Sf9 cells).[2,3] After production, rAAVs are purified using a combination of affinity chromatography with anion exchange chromatography or cesium chloride (CsCl) or iodixanol density gradient ultracentrifugation (DG-UC), followed by buffer exchange and concentration to give drug substances. The rAAVs produced by these processes usually contain both full particles (FPs) that encapsidate a designed full-length genome and empty particles (EPs) that do not encapsidate the genome. They also sometimes contain partial particles (PPs) that encapsidate an incomplete genome or overpackaged particles (OPs) that encapsidate longer length or larger number of genomes than FPs. These particles, apart from FPs, are considered product-related impurities and must be removed; however, it is difficult to completely remove the impurity particles because their outer shells (i.e., capsid) are almost identical to that of the FPs.

Several studies have investigated improving the percentage contribution of FPs to the total particles in the production stage and the genomic titer in the upstream process. The virus titer, capsid content, and aggregation are considered critical quality attributes in the rAAV production stage.[4] One study showed that the ratio of the three plasmids (pAAV-GOI, pAAV-RepCap, and pHelper) used for rAAV production influenced the genomic titer and full capsid ratio.[5] Another report revealed there were five critical parameters that greatly affected the prepurification vector quantity: the transfection

Received: February 6, 2025
Revised: April 24, 2025
Accepted: April 25, 2025
Published: May 6, 2025

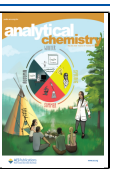





https://doi.org/10.1021/acs.analchem.5c00793
*Anal. Chem.* 2025, 97, 10405−10416

pH, production pH, complexation time, viable cell density at transfection, and transfection reagent to DNA ratio.[6]

To advance upstream optimization, a method is required that can rapidly analyze the genomic titer and FP ratio of rAAVs without prior purification. The following methods have been reported for quantifying the particles, especially EPs and FPs, in rAAV solutions:[7,8] ultraviolet−visible spectroscopy measuring the ratio of the absorbance at 260 nm to that at 280 nm, combination of enzyme-linked immunosorbent assay (ELISA) with the polymerase chain reaction (PCR), size exclusion chromatography coupled with multiangle light scattering, equilibrium density gradient or sedimentation velocity analytical ultracentrifugation,[9−11] cryogenic electron microscopy,[12] anion exchange chromatography,[13] charge detection mass spectrometry,[14,15] and mass photometry (MP).[16,17] However, with most of these methods, it is difficult to accurately quantify the content of each particle in the unpurified rAAVs, that is, rAAV in cell lysates containing many types of proteins and nucleic acids. This is because impurities interfere with the detection of rAAV particles. Small-scale purification using poly(styrene-divinylbenzene) beads (POROS CaptureSelect AAV9 Affinity Resin) has been conducted to quantify rAAV in crude materials.[18] Dual fluorescence-linked immunosorbent assay (dFLISA) enables quantification of FPs and EPs on a single plate, and can successfully quantify the genomic titer and capsid titer of rAAV in crude cell lysates.[19] However, ELISA-based methods, including dFLISA assays, take at least 2−3 h and require standard materials, and it is not easy to distinguish FPs, PPs, and OPs. MP can be used to observe single molecules on the basis of interference scattering microscopy, which typically detects single molecules that bind to glass surfaces as dark spots with negative values of interference contrast, but can also detect unbinding molecules as bright spots.[20]

Here, we propose a direct identification and quantification method for rAAV in crude cell lysate and conditioned medium by detection of unbinding particles using MP. The crude cell lysate used was a culture medium containing post-transfected cells producing rAAV to which lysis buffer containing a surfactant was added. The conditioned medium was culture medium containing transfected cells, which was collected directly during rAAV production without any processing, such as centrifugation or filtration.

## EXPERIMENTAL SECTION

**Preparation for Nontransfected Cell Lysate and Conditioned Medium.** HEK293F cells (Viral Production Cells 2.0; Thermo Fisher Scientific, Waltham, MA) were cultured in BalanCD HEK293 medium (FUJIFILM Irvine Scientific, Santa Ana, CA) with 6 mM L-glutamine (FUJIFILM, Tokyo, Japan). The medium containing cultured cells was collected directly without any processing, such as centrifugation or filtration, and used as the nontransfected conditioned medium. The nontransfected cell lysate was prepared by adding cell lysis reagent to the nontransfected conditioned medium.

**Preparation for Purified rAAV and rAAV in Crude Cell Lysate and Conditioned Medium.** rAAV serotype 2 (rAAV2) was produced using triple plasmid cotransfection. The plasmids pAAV-Rep2Cap2, pHelper, and pAAV-pGOI (CMV-EGFP) were cotransfected at a 1:1:1 ratio into a suspension of HEK293F cells (Viral Production Cells 2.0, Thermo Fisher Scientific, Waltham, MA) cultured at a 500 mL scale. After 96 h, the transfected cells were centrifuged, and the precipitates were lysed. A portion of the lysed precipitate was used for direct analysis as the crude cell lysate during rAAV production. The remaining cell lysate was filtered through a 0.22-$\mu$m filter. The filtered rAAV was purified using affinity chromatography with a POROS GoPure AAVX prepacked column (Thermo Fisher Scientific). Subsequently, a first cycle of CsCl DG-UC was performed to separate FPs and EPs. To remove the few remaining EPs mixed with FPs, the virus band containing concentrated FPs from the first CsCl DG-UC cycle was fractionated and subjected to a second cycle of CsCl DG-UC. Finally, FPs and EPs were dialyzed into 1× phosphate-buffered saline (PBS) supplemented with 200 mM NaCl and 0.001% poloxamer 188 at pH 7.4. Poloxamer 188 (Kolliphor P 188 Bio; P188) was a gift from BASF (Ludwigshafen, Germany).

rAAV serotype 8 (rAAV8), rAAV8 composed only of viral protein (VP) 3 (rAAV8-VP3only), and rAAV serotype 9 (rAAV9) were also produced at a 200 mL scale using triple plasmid cotransfection. In the transfection, the following plasmids were used: pAAV-Rep2Cap8 for rAAV8; pAAV-Rep2Cap8_VP3only for rAAV8-VP3only, where VP1 and VP2 start codons were mutated as reported previously;[21] and pAAV-Rep2Cap9 for rAAV9. For rAAV8 and rAAV9, a portion of the medium containing transfected cells was collected at 24, 48, and 72 h post-transfection (hpt) and used for direct analysis as the conditioned medium during rAAV production. For rAAV8, the entire medium was lysed at 72 hpt, while for rAAV8-VP3only and rAAV9, it was lysed at 96 hpt. A portion of the lysed culture medium was used for direct analysis as the crude cell lysate during rAAV production. The remaining cell lysate was purified following the same procedure as for rAAV2.

**Sample Preparation for Quantification of the F/E Ratio.** rAAV8-EP and rAAV8-FP were mixed to prepare samples with the ratio of the particle concentration of FPs to sum particle concentrations of FPs and EPs (F/E ratios) of 0%, 12.6%, 25.8%, 46.6%, 69.8%, and 100%. For analysis of purified rAAV, each sample was diluted in 1 × PBS with 200 mM NaCl and 0.001% poloxamer 188 to a final concentration of $1.0 \times 10^{12}$ cp/mL. A portion of the sample was mixed with nontransfected cell lysate at a 1:1 ratio and used for direct analysis of rAAV in cell lysate.

**Small-Scale Purification of rAAV.** The nontransfected cell lysate was filtered through a 0.22 $\mu$m filter. Each F/E ratio sample prepared with purified rAAV was diluted to $1 \times 10^{13}$ cp/mL in 1× PBS with 200 mM NaCl and 0.001% poloxamer 188. A mixture of 1.98 mL of the filtered nontransfected cell lysate and 20 $\mu$L of the F/E ratio sample was subjected to small-scale purification as follows. PORPS CaptureSelect AAVX Affinity Resin (Thermo Fisher Scientific) was added to an Acroprep Advance 96well-filter Plate (Pall, Port Washington, NY). Andrew+ (Waters, Milford, MA) and Extraction+ (Waters), controlled by OneLab Software (Waters), were used to perform automatic resin equilibration three times with 833 $\mu$L of 20 mM Tris (pH 7.6) containing 0.15 M NaCl and 0.001% poloxamer 188. rAAV capture was performed with 1970 $\mu$L of the sample. Resin washing was conducted five times with 500 $\mu$L of 20 mM Tris (pH 7.6) containing 1 M NaCl and 0.001% poloxamer 188. rAAV elution was performed with 100 $\mu$L of 0.1 M citrate (pH 2.5) containing 0.4 M L-arginine and 0.001% poloxamer 188. Neutralization was conducted with 50 $\mu$L of 1 M Tris-HCl (pH 9.0, NIPPON GENE, Toyama, Japan).


https://doi.org/10.1021/acs.analchem.5c00793
Anal. Chem. 2025, 97, 10405−10416

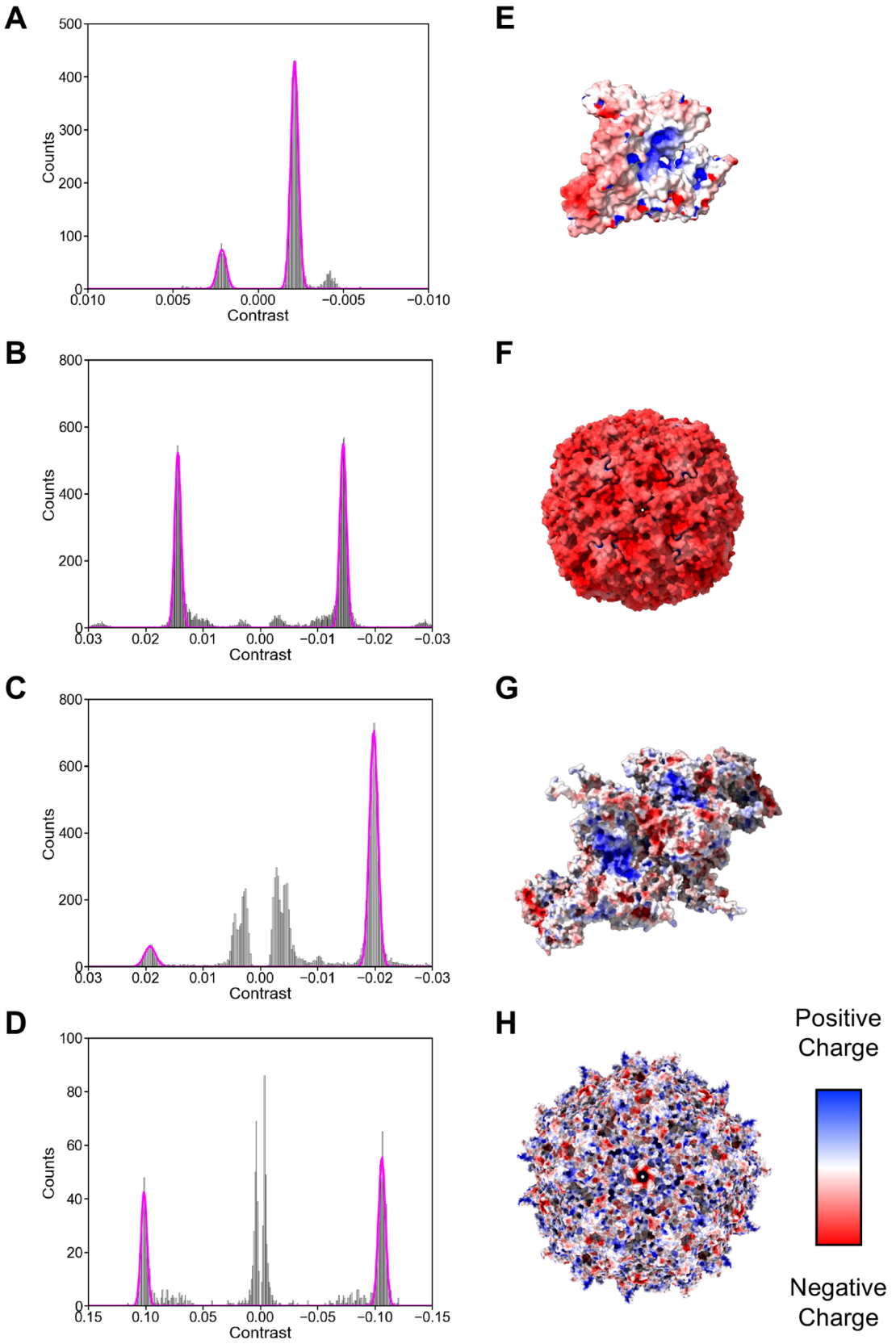


**Figure 1.** Evaluation of binding and unbinding behaviors of BSA, apoferritin, thyroglobulin, and VP3only-EP. (A) MP contrast histograms of BSA, (B) apoferritin, (C) thyroglobulin, and (D) VP3only-EP. The magenta lines represent the area of each protein on the binding and unbinding sides. (E) Electrostatic surface potential models of BSA, (F) apoferritin, (G) thyroglobulin, and (H) VP3only-EP.

**Sample Preparation for Quantification of the Genomic Titer.** The rAAV8-FP stock solution concentration was determined by digital PCR (dPCR). The solution was then diluted to $1 \times 10^{13}$ vg/mL in 1× PBS with 200 mM NaCl



https://doi.org/10.1021/acs.analchem.5c00793
Anal. Chem. 2025, 97, 10405−10416

and 0.001% poloxamer 188. For analysis of purified rAAV, the $1.0 \times 10^{13}$ vg/mL rAAV8-FP stock solution was serially diluted 2-fold. Samples for direct analysis of rAAV in the cell lysate were prepared by mixing each concentration of rAAV8-FP sample with the nontransfected cell lysate at a 1:1 ratio.

**dPCR.** Purified rAAVs were diluted in dilution buffer, which consisted of DNase I Buffer, DNase I (Takara Bio, Shiga, Japan), and 0.05 w/v% poloxamer 188, and incubated at 37 °C for 30 min. DNase I was then inactivated by adding ethylenediaminetetraacetic acid (EDTA) (pH8.0; NIPPON GENE, Tokyo, Japan) to a final concentration of 50 mM and incubated at 25 °C for 5 min and at 95 °C for 10 min. The pretreated samples were diluted with 0.001 w/v% poloxamer 188 in Tris-EDTA (NIPPON GENE, Tokyo, Japan) to the required concentration. dPCR was performed as a duplex assay using specific forward and reverse primers (900 nM) and a specific probe (250 nM) that targeted the ITR using a fluorescein amidite fluorophore (Hokkaido System Science, Hokkaido, Japan). Reaction mixes comprised primers, probes, nuclease-free water, and QuantStudio Absolute Q DNA Master Mix (Thermo Fisher Scientific). The dPCR was performed using a QuantStudio Absolute Q Digital PCR System and 16-well microfluidic array plates (Thermo Fisher Scientific). The dPCR sequence consisted of enzyme activation at 94 °C for 10 min, followed by 40 cycles of 94 °C for 5 s and 54 °C for 30 s. The following primers and probes were used: ITR forward primer 5′- GGAACCCCTAGTGATGGAGTT-3′, ITR reverse primer 5′-CGGCCTCAGTGAGCGA-3′, and ITR probe 5′-[FAM]-CACTCCCTCTCTGCGCGCTCG[BHQ1]-3′.

**Band Sedimentation Analytical Ultracentrifugation.** Band sedimentation analytical ultracentrifugation (BS-AUC) was conducted as described in our previous study.[11] Briefly, the rAAV8 samples were diluted with buffer to a UV absorbance of 0.5 at 230 nm. A 15 μL of AAV vector sample was loaded into the sample reservoir well and 15 μL of 1× PBS containing 0.001% poloxamer 188 and 200 mM NaCl was loaded into the reference reservoir well. PBS/$H_2{}^{18}O$ containing 0.001% poloxamer-188 was loaded into the sample sector (240 μL) and reference sector (250 μL). Data were collected at 20 °C using an Optima AUC at 20,000 rpm with UV detection at 230 nm. The collected data were analyzed using the analytical zone centrifugation $c(s)$ model for BS-AUC in SEDFIT (version 16.2b).[22] The lamella width, frictional ratio, meniscus, time-invariant noise, and radial-invariant noise were fitted, and a regularization level of 0.68 was used. A sedimentation coefficient range of 1−175 S was evaluated with a resolution of 350.

**MP Measurements and Analysis.** MP was conducted using a TwoMP instrument (Refeyn, Oxford, UK). Coverslips (24 × 50 mm; Thorlabs, Newton, NJ) were prepared by cleaning with Milli-Q water and ethanol. A piece of precut 2 × 3 culture well gasket (Grace Bio-Laboratories, Bend, OR) was placed onto the coverslip. For MP measurements, 16 μL of 1× PBS was loaded into the well created by the gasket, and the focus was automatically adjusted. Then, 4 μL of the sample was added to the same wells to give a final volume of 20 μL, and the samples were mixed by pipetting. Next, movie data were recorded for 60 s using AcquireMP software (version 2024 R1.1, Refeyn). The MP movie files were analyzed using DiscoverMP software (version 2024 R1, Refeyn). The AquireMP and DiscoverMP software were not modified for this study. The molecular mass of each sample was estimated from the MP contrast distribution by applying the contrast-to-mass (CTM) calibration obtained using apoferritin (catalog No. A3660; Sigma-Aldrich) and rAAV8-VP3only-EP (VP3only-EP). To evaluate binding and unbinding properties, bovine serum albumin (BSA; catalog No. A2153; Sigma−Aldrich), and thyroglobulin (catalog No. T9145; Sigma-Aldrich) were also used for CTM calibration. rAAV8-FP ($2 \times 10^{12}$ vg/mL) was prepared and analyzed before and after heating. The heated sample was incubated at 60 °C for 15 min and immediately quenched on ice. Further analysis of the mass distribution was performed using a Python script created in-house. The histograms of the mass distributions were peak fitted with a Gaussian function for EPs and FPs using the in-house Python script.

**Electrostatic Surface Potential.** The electrostatic surface potentials for BSA (PDB code: 3V03, chain A), apoferritin (PDB code: 6PXM), and VP3only-EP (PDB code: 2QA0), were calculated using their X-ray crystal structures. The structure of the VP1 unique region and VP1/VP2 common region was predicted using LocalColabfold 1.5.5[23] because of a lack of structure determination for this region. For bovine thyroglobulin, the structure was modeled using homology modeling. The MODELER 10.5 program[24] was used for the modeling, with the template as the structure of human thyroglobulin (PDB code: 6SCJ) and the sequence of bovine thyroglobulin (UniProtKB: P01267). Before the electrostatic surface was computed, the titration state of each structure was estimated and protonated in a manner consistent with favorable hydrogen bonding at pH 7 using PDB 2PQR software.[25,26] The electrostatic surfaces of these structures were calculated using Adaptive Poisson−Boltzmann Solver (APBS) software.[27] The ionic strength was set to 0.15 M.

**Calculation of the Hydrodynamic Diameter.** The radius of gyration ($R_g$) was calculated by the CRYSOL 3.2.1 program (EMBL, Hamburg, Germany)[28] using the same structure as for the calculation of electrostatic surface potential. $R_g$ was converted to hydrodynamic diameter using the formula from a previous study that $R_g$ is 0.78 times the hydrodynamic radius in a folded protein.[29]

## RESULTS AND DISCUSSION

**Binding and Unbinding Properties of the Proteins Used for Contrast-To-Mass Calibration in MP.** AcquireMP, which is a commercially available software, was used for image processing of the detected signals in MP (Figure S1). The images from five frames before and after the target frame were averaged, and a differential image was produced as a ratiometric image. Because averaging and differential processing were performed for each frame, molecules were detected as differential contrasts only when they newly bind to or unbind from the glass surface in the target frame.[20] When the rAAV solution was analyzed by MP, many bright spots with positive contrast values were observed that corresponded to unbinding events. These were in addition to dark spots with negative contrast values that corresponded to binding events (Figure S1). The binding and unbinding properties in MP contrast histograms were examined for BSA, apoferritin, thyroglobulin, and VP3only-EP (Figure 1A−D). These two proteins and two protein oligomers were used for CTM calibration for standard MP analysis according to the binding events. For BSA and thyroglobulin, few unbinding molecules were detected on the positive sites of the contrast values (Figure 1A,C), whereas for apoferritin and VP3only-EP, unbinding molecules and particles


https://doi.org/10.1021/acs.analchem.5c00793
Anal. Chem. 2025, 97, 10405−10416

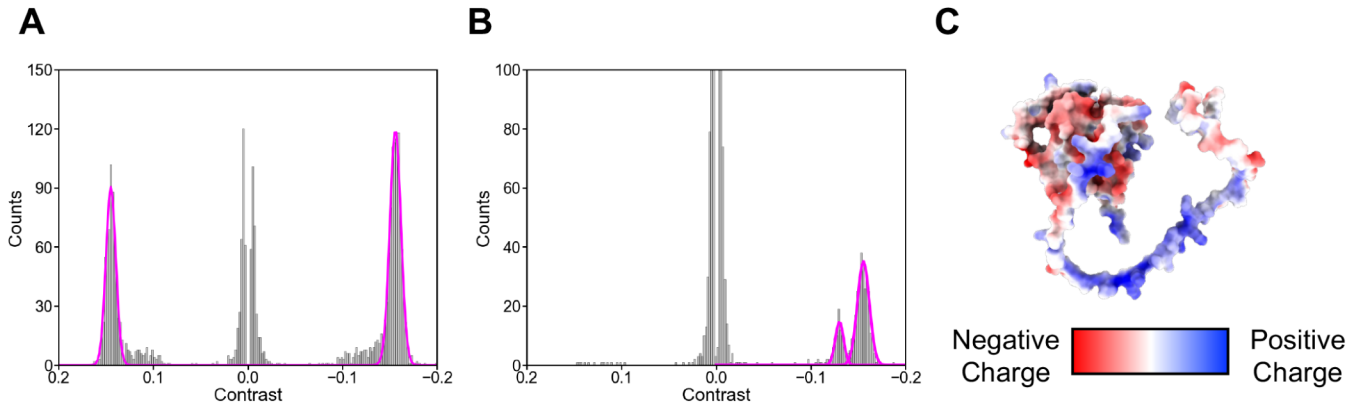


**Figure 2.** Evaluation of binding and unbinding behaviors of rAAV8-FP before and after heating. (A) MP contrast histogram of rAAV8-FP before and (B) after heating at 60 °C. The dominant peaks at contrast values of −0.156 on the binding side and 0.145 on the unbinding side before heating correspond to FPs. The peak at a contrast value of −0.130 on the binding side after heating corresponds to EPs that released the encapsidated genome. The magenta lines represent the areas of rAAV8-FP and rAAV8-EP on the binding and unbinding sides. (C) Electrostatic surface potential models of the VP1 unique region and the VP1/VP2 common region (VP1 N-terminus).

were as prevalent as binding molecules and particles with negative contrasts (Figure 1B,D).

Binding and unbinding behavior could be interpreted as protein adsorption and desorption on the surface of the glass which was used for the sample well in the MP measurement. The dominant force for protein adsorption on glass is electrostatic interactions,[30,31] but hydrophobic interactions also contribute.[31]

For BSA and thyroglobulin, the detection of few unbinding molecules suggests that the molecules strongly bind to the surface. For apoferritin and VP3only-EP, the detection of similar quantities of unbinding and binding molecules and particles suggests that the molecules and particles weakly bind to the glass surface and easily unbind from the surface. Because the surface of glass is negatively charged at pH 7.4, where MP measurements were performed,[32] positively charged molecules should bind strongly to the surface, whereas binding of negatively charged molecules will be weak. The isoelectric points of BSA, apoferritin, thyroglobulin, and VP3only-EP are 5.6, 5.9, 6.4, and 7.1, which indicates that they will all have negative net charges at pH 7.4. This implies that all the proteins should hardly bind to the glass surface. However, in the results, most molecules of BSA and thyroglobulin bind to the glass surface and did not unbind from the surface. This indicates that the binding properties of MP are not determined by the net charges of the proteins, which is consistent with a previous study that reported both the total charge and localized charge distribution of proteins changed the adsorption to the surface.[33]

The calculated charge distribution was mapped on each protein surface (Figure 1E−H). BSA, thyroglobulin, and VP3only-EP had both negative and positive regions at pH 7.4 (Figure 1E,G and H). By contrast, apoferritin was negatively charged over the entire surface (Figure 1F). Because of its negatively charged surface, apoferritin is expected to bind to the glass surface through hydrophobic interactions rather than electrostatic interactions. When apoferritin binds to the glass surface, the molecules are simultaneously repelled by electrostatic interactions, which results in the molecules becoming unbinding from the surface. For BSA and thyroglobulin, although the net charge is negative, their positively charged regions contribute to strong binding to the glass surface. A previous study showed that when proteins adsorbed to the surface, they adopted a preferential orientation with the positive charges closer to and the negative charges further away from the negatively charged surface.[34] This is also expected to occur for BSA and thyroglobulin. However, for VP3only-EP, which also has a positively charged region, unbinding particles were as prevalent as binding particles. There are different explanations for this. The typical density of silanol groups on silica surfaces is 8 sites/nm$^2$.[35] The charges on glass and silica surfaces originate from the deprotonation of silanol groups by $SiOH \rightleftharpoons SiO^- + H^+$, with a reported p$K_a$ of approximately 7.[32,36] At pH 7.4, approximately half of the silanol groups on the glass surface are deprotonated, which results in a density of approximately 4 sites/nm$^2$. BSA and thyroglobulin, which have hydrodynamic diameters of 6.7 and 17.0 nm, respectively, adopt the preferential orientation described above. This allows for contact with the glass surface only in the positively charged regions. By contrast, VP3only-EP, which has a hydrodynamic diameter of 24.8 nm, has both positively and negatively charged regions uniformly distributed across its surface. This results in contact with the glass surface through both positively and negatively charged regions (Figure S2). Consequently, VP3only-EP is simultaneously attracted to and repelled by the glass surface. This results in weak binding to the glass surface and unbinding from the surface.

Additionally, rAAV8-FP showed different binding properties before and after being heated at 60 °C. Like for VP3only-EP, before heating, unbinding particles were as prevalent as binding particles for rAAV8-FP. After heating, few unbinding particles were detected (Figure 2A,B). The detection of many unbinding particles of rAAV8-FP before heating but almost none after heating indicates that the particles weakly bind to the glass surface and easily unbind from the surface before heating. By contrast, they strongly bind to the glass surface after heating. The contrast values of rAAV before and after heating were almost the same, which indicated that the rAAV detected after heating remained assembled. In a previous study, we demonstrated that the VP1 unique region and the VP1/VP2 common region (VP1 N-terminus) were initially located inside the capsid but were exposed to the outside of the capsid after heating at 60 °C, which is below the capsid disassembly temperature.[37] Before heating, the VP1 N-terminus was located inside the capsid, which suggested that the surface charge distribution of rAAV8-FP was nearly identical to that of


https://doi.org/10.1021/acs.analchem.5c00793
Anal. Chem. 2025, 97, 10405−10416

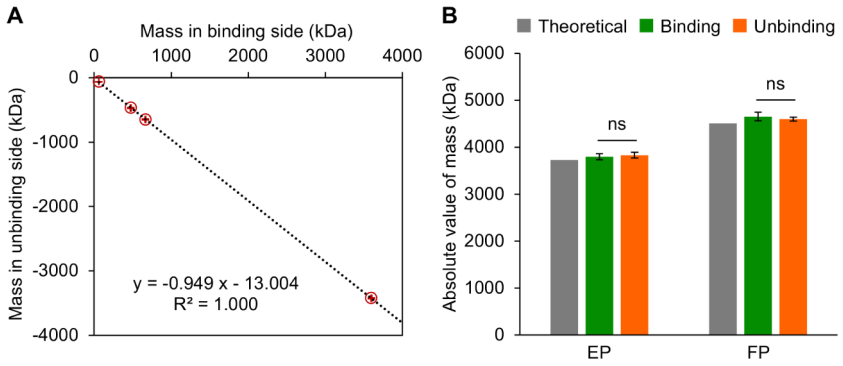


**Figure 3.** Mass calibration for unbinding events to binding events. (A) Mass plots of the binding and unbinding sides for BSA, thyroglobulin, apoferritin, and VP3only-EP using CTM calibration based on binding events. (B) Comparison of masses of theoretical values, the binding side, and the mass-calibrated unbinding side for EP and FP. The error bars represent the standard deviations of quintuplicate measurements.

VP3only-EP, with both positive and negative charges uniformly distributed. The VP1 N-terminus, which has a hydrodynamic radius of 6.6 nm, contains a positively biased region (Figure 2C). This positively charged region is exposed to the outside of the capsid after heating, which results in strong binding to the glass surface. This indicates that the binding and unbinding properties of particles (ø 25 nm) with uniformly distributed positive and negative charges can be altered by the emergence of localized positively charged regions of approximately 6.7 nm in size. Therefore, according to their localized charges and sizes, proteins can be classified into two groups in MP measurements: those that bind strongly to the glass surface and generate few unbinding molecules, and those that bind weakly to the glass surface and easily unbind from the glass surface.

MP measurements of the nontransfected HEK293 cell lysate and conditioned medium showed that higher counts of molecules with various masses were detected in the negative contrasts. For the positive contrasts, the counts were dramatically lower. The ratios of events in the positive contrasts to total events were 9.1% and 12.2% for the nontransfected cell lysate and conditioned medium, respectively (Figure S3). These results indicated that most of the proteins related to HEK293 cells belonged to the group that binds strongly to the glass surface. rAAV EPs are usually detected at approximately 0.12 and FPs at values larger than EP's contrast depending on the encapsidated single-stranded DNA length. The contrast range of the molecules detected on the unbinding side was 0 to 0.10. These values were smaller than that of the rAAV particles, which suggested that the observation of an unbinding side with positive contrast allows for detection of rAAV particles without prior purification to remove impurities from the cell lysate and conditioned medium. Therefore, we attempted to directly quantify rAAV in cell lysate and conditioned medium using the unbinding side.

**Mass Calibration for Unbinding Events to Binding Events.** In DiscoverMP, which is the standard software for analysis of MP data, CTM calibration is typically performed using binding events with negative contrasts. Because the contrast values of binding and unbinding events have the opposite sign, applying CTM calibration to binding events with negative contrasts results in positive mass values. By contrast, applying CTM calibration to unbinding events with positive contrasts results in negative mass values. However, the positive contrast for each protein is smaller than the absolute value of the negative contrast for that protein (Table S1). This results in an underestimation of absolute mass values of unbinding events. The masses obtained by applying CTM calibration to binding events are highly correlated with those obtained by applying CTM calibration to unbinding events, which are represented by proportional eqs (Figure 3A). Thus, the binding mass-to-unbinding mass calibration was applied to correct the mass of unbinding events using the eq. Consequently, the masses of EP and FP were quantified on the unbinding side with the same accuracy as on the binding side (Figure 3B). In subsequent studies, the masses of unbinding events were determined using the binding mass-to-unbinding mass calibration after CTM calibration during measurement. The masses of the unbinding events, conventionally represented as negative values because of their positive contrast, are represented as positive values in the text because negative masses are not realistic. Consequently, the histograms on the unbinding side are displayed with masses decreasing from large to small values along the *x*-axis (left to right).

**Quantification of the F/E Ratio by Detection of Unbinding Particles for rAAV in Cell Lysate.** The accuracy of quantification of the F/E ratio by direct MP measurement of rAAV in cell lysate was evaluated. Two cycles of DG-UC were performed to completely separate the EPs from FPs. BS-AUC analysis for 100% FP and 0% FP samples showed that the 100% FP sample did not contain EPs, and the 0% FP sample did not contain FPs; only peaks corresponding to FPs and EPs were observed in the 100% FP and 0% FP samples, respectively (Figure S4). Samples with F/E ratios of 100%, 69.8%, 46.6%, 25.8%, 12.6%, and 0% were prepared using purified rAAV8. Some of each sample was spiked into nontransfected cell lysate. The spiked rAAVs were analyzed by MP without prior purification. The results were compared with the F/E ratios determined for purified rAAVs and spiked rAAVs after small-scale purification using a 96-well filter plate packed with POROS CaptureSelect AAVX Affinity Resin.[38] MP mass histograms were obtained for the binding side of the purified rAAVs (Figure 4A), the binding side of the spiked rAAVs after small-scale purification (Figure 4B), and the unbinding side of the spiked rAAVs without any purification, that is, rAAVs in cell lysate (Figure 4C). For the purified rAAVs, the masses of the dominant peaks were 4,555 ± 27 kDa for the 100% FP sample and 3,799 ± 52 kDa for the 0% FP sample. For the rAAVs after small-scale purification, the masses of the dominant peaks were 4,571 ± 11 kDa for the 100% FP sample and 3,683 ± 37 kDa for the 0% FP sample. Using the mass calibration for unbinding events, the masses of the


https://doi.org/10.1021/acs.analchem.5c00793
Anal. Chem. 2025, 97, 10405−10416

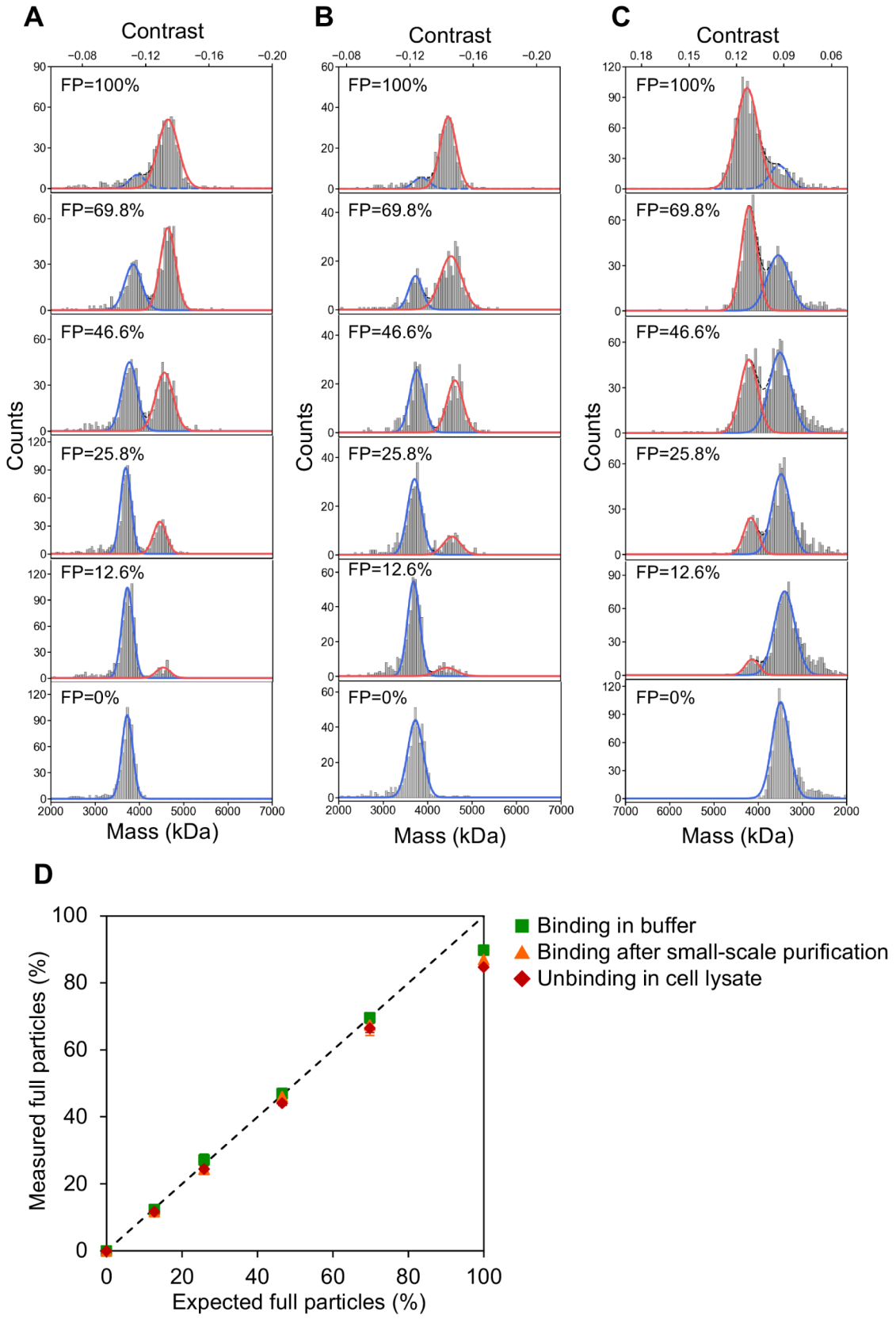


**Figure 4.** Determination of the F/E ratio. (A) MP mass histograms on the binding side at F/E ratios of 100%, 69.8%, 46.6%, 25.8%, 12.6%, and 0% in buffer. (B) The binding side after small-scale purification, and (C) the unbinding side in cell lysate. The blue lines, red lines, and blue dotted lines represent the areas of EPs, FPs, and noise components resembling EPs, respectively, according to their masses. (D) Plots of measured F/E ratios against expected values for binding rAAV in buffer, binding rAAV after small-scale purification, and unbinding rAAV in cell lysate. The error bars represent the standard deviations of triplicate measurements. The black dotted line indicates $y = x$.



https://doi.org/10.1021/acs.analchem.5c00793
*Anal. Chem.* 2025, 97, 10405−10416

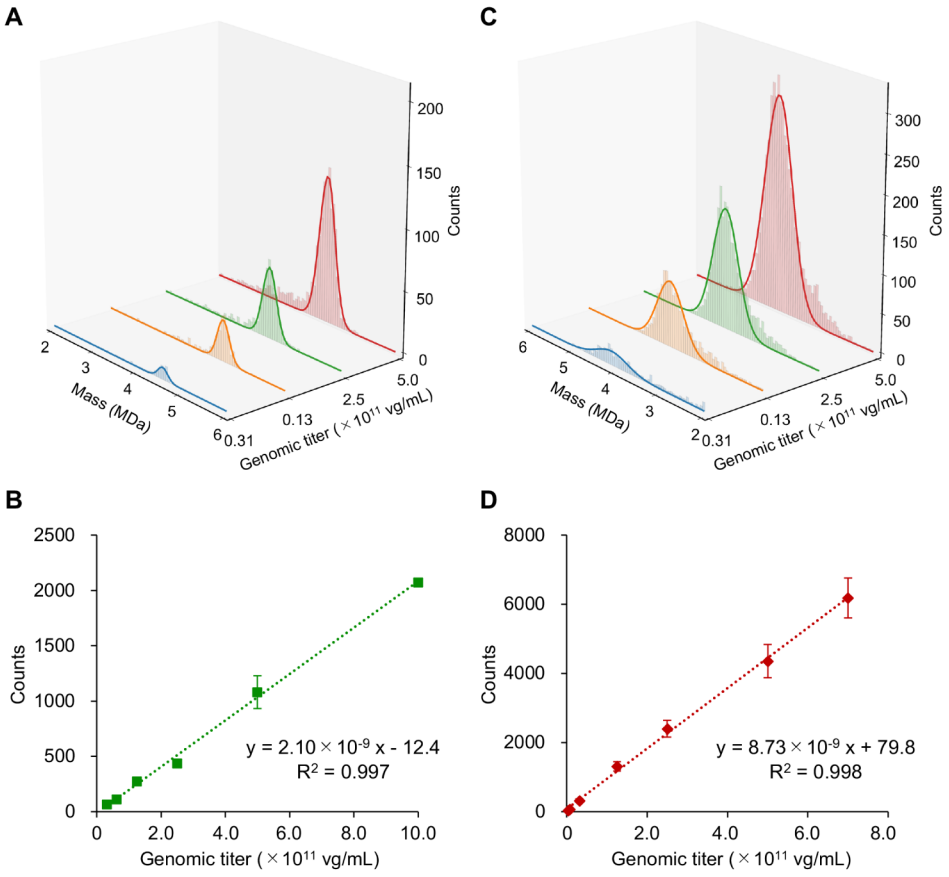


**Figure 5.** Determination of rAAV particle counts. (A) MP mass histogram on the binding side in buffer and (C) the unbinding side in cell lysate. (B) Linear correlation between rAAV-FPs and the genomic titer in purified buffer and (D) cell lysate. The error bars represent the standard deviations of quintuplicate measurements.

dominant peak for the rAAVs in the cell lysate were calculated at 4,444 ± 31 kDa for the 100% FP sample and 3,689 ± 3 kDa for the 0% FP sample. The theoretical masses of FPs and EPs used in the sample preparation were 4,508 and 3,730 kDa, respectively. Accordingly, the dominant peaks for the 100% FP and 0% FP samples were identified as FPs and EPs, respectively, with the measured values within ± 3% of the theoretical values. Thus, the established calibration successfully identified the components in the cell lysate using the unbinding side.

The F/E ratios calculated from the peak areas of FPs and EPs for the purified rAAVs showed good liner correlation (slope: 0.914, $R^2$: 0.993) (Figure 4A,D), and were similar to the values reported in previous studies.[16,17] The rAAVs after small-scale purification also showed good linear correlation (slope: 0.868, $R^2$: 0.992), which indicated that the small-scale purification caused no preferential loss of either FPs or EPs and the quantification was comparable to that for purified rAAVs (Figure 4B,D). As expected, impurities from the cell lysate interfered on the binding side for the rAAVs in cell lysate. This resulted in deviation of the F/E ratios from the expected values by more than ± 10% in samples with F/E ratios greater than 12.6% (Figure S5). However, when the unbinding side was used for the calculation, the F/E ratio was quantified with good linear correlation (slope: 0.892, $R^2$: 0.993) (Figure 4C,D). For all samples except for the 100% FP sample, the F/E ratios were quantified within ± 10% of the expected values, and the coefficient of variation (%CV) was less than 10%. These results demonstrated that the unbinding side could directly quantify the F/E ratio of rAAV in cell lysate with almost the same accuracy as purified samples and without interference from impurities. However, the peaks for FPs and EPs for rAAV in the cell lysate were broader on the unbinding side than those for purified rAAV on the binding side (Figure 4A,C). Since the peaks for purified rAAVs were not broader on the unbinding side, the components of cell lysate may influence the peak width (Figure S6). Therefore, careful identification of each particle component is required when directly quantifying samples containing PPs or OPs without purification.

A previous study showed a noise component on the left side of the dominant peak on the binding side in the TwoMP measurement.[15] A similar phenomenon was observed on both the binding side and unbinding side for the 100% FP and 0% FP samples (Figure 4A–C), with noise appearing in the region of smaller absolute mass values of the dominant peak. 100% FP sample did not contain EPs after two cycles of DG-UC purification, which was supported by BS-AUC analysis (Figure S4). However, because the noise component besides the FP peak was fitted (blue dotted lines) corresponding to the EPs, the proportion of EPs was overestimated in the 100% FP samples for all rAAVs (Figure 4A–C).

**Quantification of Genomic Titers by Detection of Unbinding Particles for rAAV in Cell Lysate.** The linearity between rAAV particle counts and concentrations was evaluated by analyzing dilutions series of purified rAAV8-FPs and rAAV8-FPs spiked into nontransfected cell lysate. The concentration of the original purified rAAV8 determined by


https://doi.org/10.1021/acs.analchem.5c00793
Anal. Chem. 2025, 97, 10405−10416

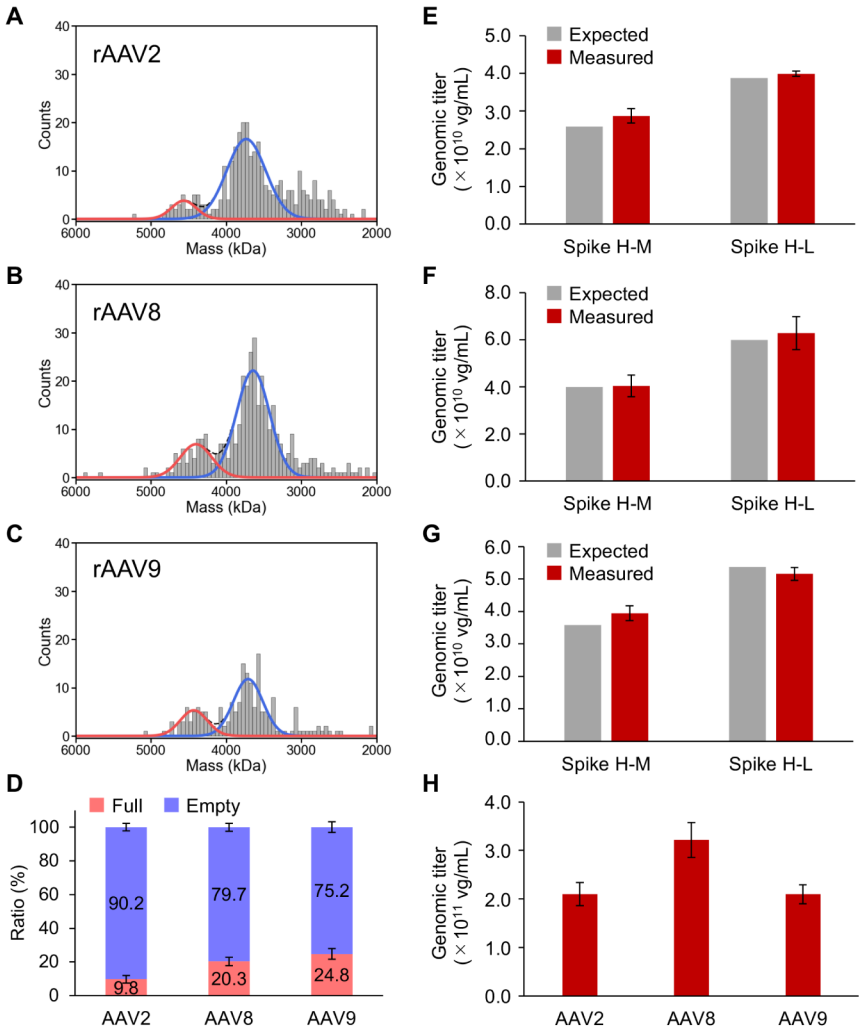


**Figure 6.** Direct quantification of rAAV2, rAAV8, and rAAV9 in crude cell lysate. (A) MP mass histogram on the unbinding side for rAAV2, (B) rAAV8, and (C) rAAV9. The blue and red lines represent the areas of EPs and FPs, respectively. (E) Genomic titers of spiked rAAV in cell lysates of rAAV2, (F) rAAV8, and (G) rAAV9. (D) F/E ratios and (H) genomic titers for rAAV2, rAAV8, and rAAV9. The error bars represent the standard deviations of triplicate measurements.

dPCR was $2.38 \times 10^{13}$ vg/mL. The rAAV particle counts in the buffer showed good linearity on the binding side with the TwoMP instrument, with a range of $3.13 \times 10^{10}$ to $1.00 \times 10^{12}$ vg/mL, $R^2$ of 0.997, and %CV within 25% (Figure 5A,B). These values are similar to those obtained in a previous study using a SamuxMP instrument.[16] We also prepared rAAV samples in cell lysate using a 1:1 mixture of purified rAAV8-FPs prediluted at serial concentrations and nontransfected cell lysate. The rAAV particle counts in the cell lysate also showed excellent linearity on the unbinding side, with a range of $3.91 \times 10^9$ to $7.00 \times 10^{11}$ vg/mL, $R^2$ of 0.998, and %CV within 25% (Figure 5C,D). These results show that MP can quantify the rAAV genomic titer in cell lysate using particle counts of the unbinding side and rAAV in buffer. Furthermore, MP exhibits higher sensitivity for rAAV in cell lysate than in buffer.

**Direct Quantification of the F/E Ratio and Genomic Titer of rAAV in Cell Lysate.** Analysis of the unbinding side demonstrated that the F/E ratio and particle count of rAAV particles spiked into nontransfected cell lysate could be quantified without purification. We applied this direct quantification method to cell lysate from actual production of rAAVs by transfection methods. Crude cell lysates of rAAV2, rAAV8, and rAAV9 were collected and prediluted 20-, 10-, and 10-fold, respectively, to the appropriate concentrations for MP. In the ratiometric images, bright spots generated by unbinding events were clearly observed on a background filled with dark spots for the many binding events, which were mainly impurities derived from the cell lysate (Figure S7). MP mass histograms of the unbinding side for rAAV2, rAAV8, and rAAV9 showed two peaks (Figure 6A–C). On the other hand, the corresponding peaks on binding side of the crude cell lysates were overlapped with the signals from impurities (Figure S8). Peaks for rAAV2, rAAV8, and rAAV9 (blue lines in Figure 6A–C) were observed 3,679 ± 45, 3,628 ± 14, and 3,672 ± 44 kDa, respectively. Peaks for rAAV2, rAAV8, and rAAV9 (red lines in Figure 6A–C) were also observed at 4,559 ± 14, 4,406 ± 24, and 4,432 ± 19 kDa, respectively. According to the masses of these peaks, the first set (blue lines) were identified as EPs and the second set (red lines) as FPs. The F/E ratios of rAAV2, rAAV8, and rAAV9 were 9.8%, 20.3%, and 24.8%, respectively (Figure 6D).

Because the counts of rAAV-FPs obtained by MP showed good linearity with the genomic titer in nontransfected lysate, we investigated spiking with purified rAAV at a known


https://doi.org/10.1021/acs.analchem.5c00793
Anal. Chem. 2025, 97, 10405−10416

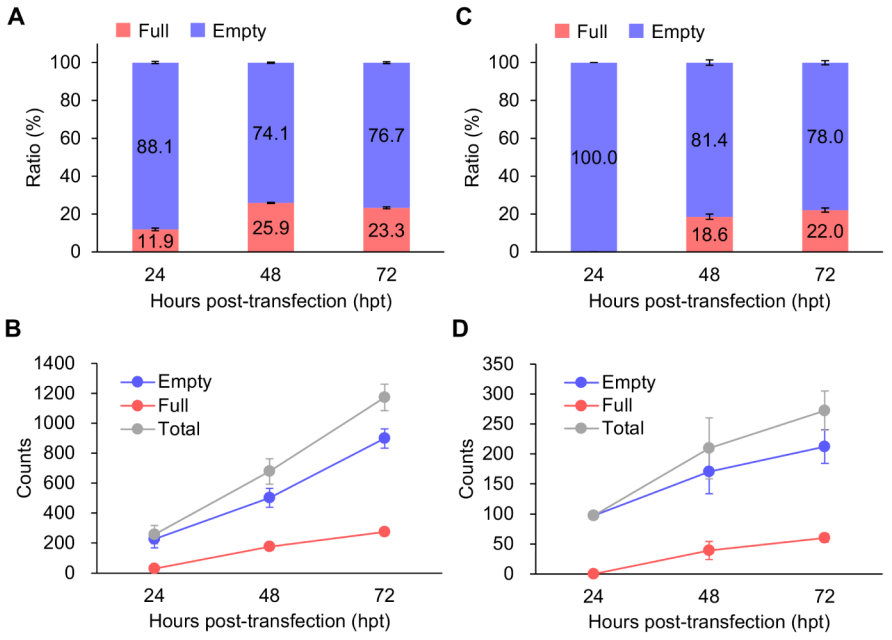


**Figure 7.** Direct quantification of rAAV8 and rAAV9 in conditioned medium during production. (A) F/E ratios at 24, 48, and 72 hpt in rAAV8 and (C) rAAV9. (B) rAAV particle counts at 24, 48, and 72 hpt in rAAV8 and (D) rAAV9. The error bars represent the standard deviations of triplicate measurements.

concentration for estimation of the unknown rAAV genomic titer in the crude cell lysate. Purified rAAV2-FPs, rAAV8-FPs, and rAAV9-FPs for spiking were prepared at three different concentrations to estimate the genomic titers. The concentration of purified rAAV2-FPs, rAAV8-FPs, and rAAV9-FPs at high concentration were determined by dPCR as $5.17 \times 10^{12}$, $4.00 \times 10^{12}$, and $3.58 \times 10^{12}$ vg/mL, respectively. Purified rAAVs at moderate and low concentrations were prepared by 2-fold serial dilution of the high concentration purified rAAVs. These purified rAAV-FPs with three different concentrations were spiked into the crude cell lysates in a 1:1 ratio. Nonspiked crude cell lysates were also prepared by adding corresponding buffer of purified rAAV-FPs in a 1:1 ratio. The spiked and nonspiked crude cell lysates was diluted 10-fold for AAV2 or 5-fold for rAAV8 and rAAV9, respectively, in 1 × PBS with 200 mM NaCl and 0.001% poloxamer 188 to the concentration in linear range of MP. The FP counts measured by MP were plotted against the expected titer of the spiked rAAV FPs to obtain the linear regression equation (Figure S9). Note that each titer on the *x*-axis is the concentration of the spiked rAAV-FPs which was further diluted 5-fold in the wells of MP measurement. The reciprocal value of the obtained slope represents the genomic titer per count. Thus, the genomic titer of rAAV in crude cell lysate was estimated from the counts of rAAV FPs that were obtained by MP. The recoveries of the spiked rAAVs were evaluated by calculating the difference between the high minus the moderate spiking concentrations (spike H−M) and the high minus the low spiking concentrations (spike H−L). For spike H−M, the recovered genomic titers of rAAV2, rAAV8, and rAAV9 were $2.87 \times 10^{10}$, $4.04 \times 10^{10}$, and $3.95 \times 10^{10}$ vg/mL, respectively. For spike H−L, the recovered genomic titers of rAAV2, rAAV8, and rAAV9 were $3.99 \times 10^{10}$, $6.28 \times 10^{10}$, and $5.16 \times 10^{10}$, respectively (Figure 6E−G). The measured values were within 20% of the expected values, which indicated that the spiking approach for estimating the genomic titers in crude samples was effective. This enabled quantification of rAAV without interference from impurities in the crude cell lysate. Therefore, applying the obtained slope of the genomic titer per count to the nonspiked crude samples, the original genomic titers, that is, prediluted and nonspiked genomic titers of rAAV2, rAAV8, and rAAV9 in the crude samples were calculated as $2.10 \times 10^{11}$, $3.21 \times 10^{11}$, and $2.10 \times 10^{11}$ vg/mL, respectively (Figure 6H).

The production scale and cell lysis conditions for rAAV2 were different from those for rAAV8 and rAAV9 in this study. Because rAAV2 predominantly accumulates in the cells during production,[5,39,40] rAAV2 was produced at a 500 mL scale, and only the cells pelleted by centrifugation were lysed up to a final volume of 200 mL. By contrast, rAAV8 and rAAV9, which are distributed both in the cells and in the culture medium,[5,39−41] were produced at a 200 mL scale and harvested by lysing the entire cell culture medium. This resulted in a final volume of 218 mL. Because of these differences, the concentration of impurities derived from the cell lysate in rAAV2 samples was approximately 2.5 times that in the rAAV8 and rAAV9 samples. These impurities made it difficult to directly observe rAAV2 in crude cell lysate. However, under our production conditions, rAAV2 itself was enriched. This allowed for detection by MP using a high dilution factor of crude cell lysate to minimize interference from the impurities. Therefore, direct quantification by MP is feasible regardless of differences in the cell lysis conditions between rAAV2 and rAAV8/rAAV9 when rAAVs are produced in sufficient quantities. In the initial measurement for direct quantification of rAAV, several diluted crude samples should be measured to determine the dilution factor at which rAAV in the crude sample falls within the linear range of MP. Direct quantification by MP has the potential to be applied to various serotypes, irrespective of the tendency of rAAV to accumulate within the cells or be released into the culture medium.

**Monitoring of the F/E Ratio and rAAV Particle Counts in Conditioned Medium in rAAV Production.** The use of the unbinding side suggested that unbinding rAAV could be


https://doi.org/10.1021/acs.analchem.5c00793
Anal. Chem. 2025, 97, 10405−10416

detected without any purification, not only in cell lysate but also in conditioned medium (Figure S3). Consequently, we tried to confirm that rAAV in conditioned medium could be directly quantified. Conditioned media from rAAV8 and rAAV9, which were predominantly released into the culture medium, were collected and directly quantified at 24, 48, and 72 hpt. The collected conditioned media of rAAV8 and rAAV9 were then prediluted 6- and 5-fold, respectively, to achieve the appropriate concentrations for MP. MP mass histograms of the conditioned medium exhibited one or two distinct peaks (Figure S10). The peaks were identified as EPs (blue lines) and FPs (red lines) according to mass values obtained using calibration of the binding mass to the unbinding mass after CTM calibration during the measurement. For rAAV8, the F/E ratio was higher at 48 hpt than at 72 hpt (Figure 7A). However, the FP count increased over time (Figure 7B). For rAAV9, both the FP count and the F/E ratio increased over time (Figure 7C,D). For the conditioned medium of rAAV8 at 72 hpt, genomic titer estimation using the spiking approach described above resulted in a value of $2.30 \times 10^{11}$ vg/mL. Compared with the cell lysate collected at 72 hpt, the F/E ratios of the cell lysate and the conditioned medium were not significantly different ($p = 0.217$). By contrast, the genomic titer in the conditioned medium was 71.7% of that in the cell lysate. The lack of difference in the F/E ratio between the cell lysate and the conditioned medium indicates that neither EPs nor FPs are preferentially released into the culture medium. In previous studies, 70%−85% of rAAV8 was released into the conditioned medium,[39,41] which is consistent with our results. These results demonstrate that our method can be used to quantify the F/E ratio and genomic titer of rAAV in conditioned medium without any purification.

## CONCLUSIONS

We successfully identified FPs and EPs using the mass of each peak and quantified the F/E ratio and genomic titer of rAAV in cell lysate and conditioned medium using MP without prior purification. We focused on the difference in binding and unbinding properties of rAAVs and other impurities in the cell lysate and conditioned medium in MP detection. The signal of the unbinding side was used to overcome any interference from impurities. By analyzing the unbinding side of the histogram, the F/E ratio of rAAV in the cell lysate was directly quantified with accuracy and linearity comparable to that of purified rAAV. The particle counts of the unbinding side were highly correlated to the expected genomic titer, which led to direct estimation of the genomic titer of rAAV in cell lysate. The established method was applied to three AAV serotypes, AAV2, AAV8, and AAV9, in crude cell lysate, and used to determine the F/E ratios and estimate the genomic titers. This method shows potential for application to various serotypes that accumulate within cells or are released into the culture medium. Changes over time were observed for the F/E ratios of rAAVs in conditioned medium during the manufacturing process. These results show that direct quantification by MP is a convenient, rapid, and accurate method for quantifying unpurified rAAV with a small sample amount. This method will be useful for improving the rAAV production process, for example, by screening of production conditions.

## ASSOCIATED CONTENT

### Supporting Information

The Supporting Information is available free of charge at https://pubs.acs.org/doi/10.1021/acs.analchem.5c00793.

Additional figures explaining rAAV quantification by MP (PDF)

## AUTHOR INFORMATION


### Corresponding Author

**Susumu Uchiyama** − *Department of Biotechnology, Graduate School of Engineering, The University of Osaka, Suita, Osaka 565-0871, Japan;* orcid.org/0000-0002-5181-179X; Email: suchi@bio.eng.osaka-u.ac.jp

### Authors

**Yuki Yamaguchi** − *Department of Biotechnology, Graduate School of Engineering, The University of Osaka, Suita, Osaka 565-0871, Japan;* orcid.org/0000-0001-7856-4031

**Saki Shimojo** − *Department of Biotechnology, Graduate School of Engineering, The University of Osaka, Suita, Osaka 565-0871, Japan*

**Risa Shibuya** − *Department of Biotechnology, Graduate School of Engineering, The University of Osaka, Suita, Osaka 565-0871, Japan;* orcid.org/0000-0002-1337-9334

**Karin Bandoh** − *Department of Biotechnology, Graduate School of Engineering, The University of Osaka, Suita, Osaka 565-0871, Japan*

**Aoba Matsushita** − *U-Medico Inc., Suita, Osaka 565-0871, Japan*

**Mitsuko Fukuhara** − *Department of Biotechnology, Graduate School of Engineering, The University of Osaka, Suita, Osaka 565-0871, Japan; U-Medico Inc., Suita, Osaka 565-0871, Japan*

**Yasuo Tsunaka** − *Department of Biotechnology, Graduate School of Engineering, The University of Osaka, Suita, Osaka 565-0871, Japan;* orcid.org/0000-0002-7366-7610

**Tetsuo Torisu** − *Department of Biotechnology, Graduate School of Engineering, The University of Osaka, Suita, Osaka 565-0871, Japan;* orcid.org/0000-0002-8269-7803

Complete contact information is available at: https://pubs.acs.org/10.1021/acs.analchem.5c00793


### Author Contributions

#Y.Y. and S.S. contributed equally. Conceptualization, Y.Y., S.S., and S.U.; Investigation, S.S., R.S., and K.B.; Resources, A.M., M.F., and Y.T.; Visualization, S.S.; Writing − original draft, Y.Y., S.S., and S.U.; Writing − review and editing, Y.Y., S.S., T.T. and S.U.

### Notes

The authors declare the following competing financial interest(s): The authors declare the following financial interests/personal relationships that may be considered as potential competing interests: Aoba Matsushita and Mitsuko Fukuharas relationship with U-Medico Inc. that includes employment; Susumu Uchiyamas relationship with U-Medico Inc. that includes founder, shareholder, and CSO.

## ACKNOWLEDGMENTS

This study was supported by Grants-in-Aid from the 'Research and Development of Core Technologies for Gene and Cell Therapy' supported by Japan Agency for Medical Research and Development (AMED) [grant numbers JP18ae0201001 and

JP24se0123004h0101]. Computations were partially performed on the NIG supercomputer at ROIS National Institute of Genetics. We thank Gabrielle David, PhD, from Edanz (https://jp.edanz.com/ac) for editing the English text of a draft of this manuscript.

## REFERENCES

(1) Wang, J.-H.; Gessler, D. J.; Zhan, W.; Gallagher, T. L.; Gao, G. *Signal Transduct. Target. Ther.* **2024**, *9* (1), 78.
(2) Gray, S. J.; Choi, V. W.; Asokan, A.; Haberman, R. A.; McCown, T. J.; Samulski, R. J. *Curr. Protoc. Neurosci.* **2011**, *4* (1), 4−17.
(3) Xiao, X.; Li, J.; Samulski, R. J. *J. Virol.* **1998**, *72* (3), 2224−2232.
(4) Gimpel, A. L.; Katsikis, G.; Sha, S.; Maloney, A. J.; Hong, M. S.; Nguyen, T. N. T.; Wolfrum, J.; Springs, S. L.; Sinskey, A. J.; Manalis, S. R.; Barone, P. W.; Braatz, R. D. *Mol. Ther. Methods Clin. Dev.* **2021**, *20*, 740−754.
(5) Park, S.; Shin, S.; Lee, H.; Jang, J.-H.; Lee, G. M. *Biotechnol. J.* **2024**, *19* (3), No. e2300667.
(6) Coplan, L.; Zhang, Z.; Ragone, N.; Reeves, J.; Rodriguez, A.; Shevade, A.; Bak, H.; Tustian, A. D. *Biotechnol. Prog.* **2024**, *40* (3), No. e3445.
(7) Werle, A. K.; Powers, T. W.; Zobel, J. F.; Wappelhorst, C. N.; Jarrold, M. F.; Lyktey, N. A.; Sloan, C. D. K.; Wolf, A. J.; Adams-Hall, S.; Baldus, P.; Runnels, H. A. *Mol. Ther. Methods Clin. Dev.* **2021**, *23*, 254−262.
(8) Richter, K.; Wurm, C.; Strasser, K.; Bauer, J.; Bakou, M.; VerHeul, R.; Sternisha, S.; Hawe, A.; Salomon, M.; Menzen, T.; Bhattacharya, A. *Eur. J. Pharm. Biopharm.* **2023**, *189*, 68.
(9) Hirohata, K.; Yamaguchi, Y.; Maruno, T.; Shibuya, R.; Torisu, T.; Onishi, T.; Chono, H.; Mineno, J.; Yuzhe, Y.; Higashiyama, K.; Masumi-Koizumi, K.; Uchida, K.; Yamamoto, T.; Uchida, E.; Okada, T.; Uchiyama, S. *Anal. Chem.* **2024**, *96* (2), 642−651.
(10) Maruno, T.; Usami, K.; Ishii, K.; Torisu, T.; Uchiyama, S. *J. Pharm. Sci.* **2021**, *110* (10), 3375−3384.
(11) Maruno, T.; Ishii, K.; Torisu, T.; Uchiyama, S. *J. Pharm. Sci.* **2023**, *112* (4), 937−946.
(12) Nishiumi, H.; Hirohata, K.; Fukuhara, M.; Matsushita, A.; Tsunaka, Y.; Rocafort, M. A. V.; Maruno, T.; Torisu, T.; Uchiyama, S. *J. Pharm. Sci.* **2024**, *113*, 1804−1815.
(13) Fu, X.; Chen, W.-C.; Argento, C.; Clarner, P.; Bhatt, V.; Dickerson, R.; Bou-Assaf, G.; Bakhshayeshi, M.; Lu, X.; Bergelson, S.; Pieracci, J. *Hum. Gene Ther: Methods* **2019**, *30* (4), 144−152.
(14) Wörner, T. P.; Snijder, J.; Friese, O.; Powers, T.; Heck, A. J. R. *Mol. Ther. Methods Clin. Dev.* **2022**, *24*, 40−47.
(15) Nakatsuka, R.; Yamaguchi, Y.; Hirohata, K.; Shimojo, S.; Murakami, M.; Rocafort, M. A. V.; Tsunaka, Y.; Fukuhara, M.; Torisu, T.; Uchiyama, S. *Anal. Chem.* **2024**, *96* (42), 17037−17046.
(16) Wagner, C.; Fuchsberger, F. F.; Innthaler, B.; Lemmerer, M.; Birner-Gruenberger, R. *Int. J. Mol. Sci.* **2023**, *24* (13), 11033.
(17) Wu, D.; Hwang, P.; Li, T.; Piszczek, G. *Gene Ther.* **2022**, *29* (12), 691−697.
(18) Wagner, C.; Fuchsberger, F. F.; Innthaler, B.; Pachlinger, R.; Schrenk, I.; Lemmerer, M.; Birner-Gruenberger, R. *Int. J. Mol. Sci.* **2024**, *25* (2), 838.
(19) Soth, S.; Takakura, M.; Suekawa, M.; Onishi, T.; Hirohata, K.; Hashimoto, T.; Maruno, T.; Fukuhara, M.; Tsunaka, Y.; Torisu, T.; Uchiyama, S. *Mol. Ther. Methods Clin. Dev.* **2024**, *32* (3), 101291.
(20) Young, G.; Hundt, N.; Cole, D.; Fineberg, A.; Andrecka, J.; Tyler, A.; Olerinyova, A.; Ansari, A.; Marklund, E. G.; Collier, M. P.; Chandler, S. A.; Tkachenko, O.; Allen, J.; Crispin, M.; Billington, N.; Takagi, Y.; Sellers, J. R.; Eichmann, C.; Selenko, P.; Frey, L.; Riek, R.; Galpin, M. R.; Struwe, W. B.; Benesch, J. L. P.; Kukura, P. *Science* **2018**, *360* (6387), 423−427.
(21) Warrington, K. H., Jr.; Gorbatyuk, O. S.; Harrison, J. K.; Opie, S. R.; Zolotukhin, S.; Muzyczka, N. *J. Virol.* **2004**, *78* (12), 6595−6609.
(22) Schuck, P. *Biophys. J.* **1998**, *75* (3), 1503−1512.
(23) Mirdita, M.; Schütze, K.; Moriwaki, Y.; Heo, L.; Ovchinnikov, S.; Steinegger, M. *Nat. Methods* **2022**, *19* (6), 679−682.
(24) Eswar, N.; Webb, B.; Marti-Renom, M. A.; Madhusudhan, M. S.; Eramian, D.; Shen, M.-Y.; Pieper, U.; Sali, A. *Curr. Protoc. Bioinformatics* **2006**, *5* (1), 5−6.
(25) Dolinsky, T. J.; Nielsen, J. E.; McCammon, J. A.; Baker, N. A. *Nucleic Acids Res.* **2004**, *32*, W665−W667.
(26) Dolinsky, T. J.; Czodrowski, P.; Li, H.; Nielsen, J. E.; Jensen, J. H.; Klebe, G.; Baker, N. A. *Nucleic Acids Res.* **2007**, *35*, W522−W525.
(27) Jurrus, E.; Engel, D.; Star, K.; Monson, K.; Brandi, J.; Felberg, L. E.; Brookes, D. H.; Wilson, L.; Chen, J.; Liles, K.; Chun, M.; Li, P.; Gohara, D. W.; Dolinsky, T.; Konecny, R.; Koes, D. R.; Nielsen, J. E.; Head-Gordon, T.; Geng, W.; Krasny, R.; Wei, G.-W.; Holst, M. J.; McCammon, J. A.; Baker, N. A. *Protein Sci.* **2018**, *27* (1), 112−128.
(28) Franke, D.; Petoukhov, M. V.; Konarev, P. V.; Panjkovich, A.; Tuukkanen, A.; Mertens, H. D. T.; Kikhney, A. G.; Hajizadeh, N. R.; Franklin, J. M.; Jeffries, C. M.; et al. *J. Appl. Crystallogr.* **2017**, *50* (4), 1212−1225.
(29) Nygaard, M.; Kragelund, B. B.; Papaleo, E.; Lindorff-Larsen, K. *Biophys. J.* **2017**, *113* (3), 550−557.
(30) Duncan, M. *Int. J. Pharm.* **1995**, *120* (2), 179−188.
(31) Yoneda, S.; Maruno, T.; Mori, A.; Hioki, A.; Nishiumi, H.; Okada, R.; Murakami, M.; Zekun, W.; Fukuhara, A.; Itagaki, N.; Harauchi, Y.; Adachi, S.; Okuyama, K.; Sawaguchi, T.; Torisu, T.; Uchiyama, S. *J. Pharm. Sci.* **2021**, *110* (11), 3568−3579.
(32) Behrens, S. H.; Grier, D. G. *J. Chem. Phys.* **2001**, *115* (14), 6716−6721.
(33) Gong, P.; Szleifer, I. *J. Colloid Interface Sci.* **2004**, *278* (1), 81−90.
(34) Carlsson, F.; Hyltner, E.; Arnebrant, T.; Malmsten, M.; Linse, P. *J. Phys. Chem. B* **2004**, *108* (28), 9871−9881.
(35) Zhao, C.; Ebeling, D.; Siretanu, I.; van den Ende, D.; Mugele, F. *Nanoscale* **2015**, *7* (39), 16298−16311.
(36) Secreast, S. L. *J. Chromatogr. A* **1991**, *544*, 99−111.
(37) Yamaguchi, Y.; Shimojo, S.; Ikeda, T.; Fukuhara, M.; Tsunaka, Y.; Shibuya, R.; Rocafort, M. A. V.; Nakatsuka, R.; Hirohata, K.; Torisu, T.; et al. *Mol. Ther. Methods Clin. Dev.* **2025**, 101480.
(38) Florea, M.; Nicolaou, F.; Pacouret, S.; Zinn, E. M.; Sanmiguel, J.; Andres-Mateos, E.; Unzu, C.; Wagers, A. J.; Vandenberghe, L. H. *Mol. Ther. Methods Clin. Dev.* **2023**, *28*, 146−159.
(39) Vandenberghe, L. H.; Xiao, R.; Lock, M.; Lin, J.; Korn, M.; Wilson, J. M. *Hum. Gene Ther.* **2010**, *21* (10), 1251−1257.
(40) Lock, M.; Alvira, M.; Vandenberghe, L. H.; Samanta, A.; Toelen, J.; Debyser, Z.; Wilson, J. M. *Hum. Gene Ther.* **2010**, *21* (10), 1259−1271.
(41) Piras, B. A.; Drury, J. E.; Morton, C. L.; Spence, Y.; Lockey, T. D.; Nathwani, A. C.; Davidoff, A. M.; Meagher, M. M. *Mol. Ther. Methods Clin. Dev.* **2016**, *3* (16015), 16015.


https://doi.org/10.1021/acs.analchem.5c00793
*Anal. Chem.* 2025, 97, 10405−10416